JOURNAL OF NEUROTRAUMA 28:1229–1236 (July 2011)

DOI: 10.1089/neu.2011.1832

Novel Model to Investigate Blast Injury in the Central Nervous System

Sean Connell,[1] Jian Gao,[3] Jun Chen,[3] and Riyi Shi[1,2]

Abstract

Blast-induced neurotrauma (BINT) is a common injury modality associated with the current war efforts and increasing levels of terrorist activity. Exposure to the primary blast wave generated by explosive devices causes significant neurological deficits and is responsible for many of the war-related pathologies. Despite research efforts, the mechanism of injury is still poorly understood. To this end, we have established a novel *ex vivo* model for the direct observation and quantification of BINT at the tissue level. The model provides a quantifiable and reproducible method to illustrate the mechanism of BINT. Isolated sections of guinea pig spinal cord white matter were exposed to a supersonic shockwave using a blast generator with small-scaled explosives. The blast wave impact with isolated tissue was observed using focused shadowgraphy with a high-speed camera recording at 90,000 fps. Concurrently, functional deficits were measured by monitoring the production of compound action potentials using a double sucrose gap-recording chamber. Additionally, anatomical deficits were measured after blast exposure with a dye exclusion assay to visualize axonal membrane permeability. Our findings demonstrate that direct exposure to the blast wave compressed nervous tissue at a rate of 60 m/sec and led to significant functional deficits. Damage to the isolated spinal cord was marked by increased axonal permeability, suggesting rapid compression from the shockwave-generated high strain rates that resulted in membrane disruption. The model provides new insight into the mechanism of BINT and permits direct observation that may contribute to the development of appropriate treatment regimens.

Key words: axolemma; axonal injury; electrophysiology; military injury; neuronal cell death

Introduction

BLAST INJURY is considered the signature wound of the current military conflicts. The increasing prevalence of blast injury can be attributed to the more frequent use of explosive devices in combat and improved blast survival rates offered by modern body armor. Currently, over two-thirds of military injuries are caused by blasts (Coupland and Meddings, 1999; Warden, 2006). Despite its importance, the mechanism of injury is still poorly understood.

Classical understanding of blast injury focused on air-filled organs (i.e., gastrointestinal tract, lungs, and ears), as these systems were historically considered the most susceptible to pressure variations created by the explosion (Clemedson, 1956). However, recent evidence suggests that exposure to the primary blast wave causes permanent or transient brain damage, indicating that the central nervous system is vulnerable to blast injury with potentially devastating consequences. Recent evidence provided by case reports and experimental animal models demonstrate that the central nervous system is highly susceptible to injury from blast exposure (Kocsis and Tessler, 2009; Okie, 2005; Warden et al., 2009). For instance, soldiers exposed to blasts without external signs of injury experience cognitive deficits attributed to traumatic brain injury (Kocsis and Tessler, 2009; Okie, 2005; Warden et al., 2009). Experimental animal models of blast exposure using shock tubes have shown anatomical alterations marked by histological changes in the central nervous system, including myelin disruption and neuronal degeneration, with increases in oxidative stress (Cernak et al., 2001a, 2001b; Saljo et al., 2002). Still other studies have shown impaired performance after exposure on active avoidance tests and behavioral changes with passive learning paradigms, indicating onset of long-term deficits (Moochhala et al., 2004). Consistent with such observations, the direct intracranial recording of a pressure wave during blast exposure indicates that the shockwave is capable of penetrating the skull (Chavko et al., 2007).

[1]Weldon School of Biomedical Engineering, [2]Department of Basic Medical Sciences, School of Veterinary Medicine, and [3]School of Mechanical Engineering, Purdue University, West Lafayette, Indiana.

Despite indirect evidence, direct observation of the blast wave impact and the deformation of nervous tissue in response to blast loading have not been recorded. The degree of deformation and rate of compression of nervous tissue are both known factors crucial for determining the severity of damage (LaPlaca et al., 1997; Shi and Blight, 1996; Shi and Whitebone, 2006; Shi, 2004). This information is indispensible to demonstrate directly that primary blast exposure alone is capable of producing significant brain injury. Furthermore, understanding the tissue level reaction to blast exposure is necessary for defining failure criteria to appropriately diagnose blast-induced neurotrauma (BINT) and provide a measure for developing protective equipment.

Therefore, the objective of this study was to establish a model that allows for the direct observation and quantification of BINT. Furthermore, we intend to use this model to correlate deformation and functional outcomes of blast exposure on the central nervous system. To this end, we have established a small-scale BINT model that allows for direct observation of blast injury at the tissue level. Our model provides the capability to directly record the detailed events of primary injury and separate the primary event from secondary systemic responses, specifically isolating the effects of blast wave exposure. In addition, physical characteristics of the blast wave, mechanical deformation of the tissue, and consequential functional and structural damage can be recorded with the same tissue sample. Velocity of the blast wave and the rate and degree of tissue deformation were measured using a high-speed shadowgraph technique. Subsequently, the forces produced by blast exposure were correlated with observed functional and anatomical deficits to illuminate the mechanism of injury. Such information provides a clinically relevant tool for determining the severity of injury in response to degree of blast exposure.

Methods

Spinal cord isolation

Experimental protocols used in this study were reviewed and approved by the Purdue University Animal Care and Use Committee. All animals were handled in agreement with the National Institutes of Health Guide for the Care and Use of Laboratory Animals in order to reduce animal discomfort.

Adult female guinea pigs (250–350 g) were anesthetized (ketamine 60 mg/kg and xylazine 10 mg/kg) and perfused with cold oxygenated Krebs solution (124 mM NaCl, 5 mM KCl, 1.2 mM KH_2PO_4, 1.3 mM $MgSO_4$, 2 mM $CaCl_2$ 20 mM dextrose, 26 mM $NaHCO_3$, and 10 mM sodium ascorbate) to reduce core body temperature and remove blood. The vertebral column was removed and a complete laminectomy was performed to expose the spinal cord. Ventral white matter was isolated, similarly to previously described techniques as shown in Figure 1 (Shi, 2004). To allow recovery, ventral white matter strips were placed in continuously oxygenated Krebs solution immediately following the procedure.

Blast injury experimental set-up

Explosive blast injury was created using 2.5-cm strips of shock tubing (Nonel lead line with an explosive lining of 0.1 grain/foot composed of tetranitramine and aluminum) remotely detonated with a custom initiator (300V plasma discharge pulse generator). The resultant explosion and shockwave were directed through a hollow aluminum blast nozzle (8 cm in length with 0.6 cm diameter) on an isolated section of white matter secured directly beneath the event in a double-sucrose gap recording chamber.

Testing the physiological response of nervous tissue to various blast loading events was accomplished by adjusting the distance between the spinal cord and the blast nozzle. Blast intensity decreases as the distance from the blast epicenter increases, according to Hopkinson's rule. Severe exposure was designated as 1.25 cm from the spinal cord, while moderate exposure was 1.5 cm, and mild exposure was 1.75 cm to achieve a dose-response.

Overpressure measurements were obtained using a dynamic pressure transducer (Omega DPX101; Omega Engineering, Stamford, CT). Total pressure (including static pressure due to thermal motion and dynamic pressure from the net air motion impacting the sensor) of the blast at each level were recorded using a pressure transducer mounted normal to the shockwave.

Shadowgraph technique

Imaging the developing shockwave and resultant tissue deformation was accomplished using focused shadowgraphy. The shadowgraph technique captures refraction of light rays as they pass through a disturbance such as a shockwave. Resultant changes in light intensity are proportional to the refractive index of rays passing through the inhomogeneities. The image captured is therefore a shadow of the disturbance (Settles, 2001).

Continuous light supplied from a 15 mW He-Ne laser was attenuated with a neutral density filter and collimated using a spatial filter and doublet (f = 200 mm). Parallel rays of light were directed through the emergent shockwave. Refracted light exiting the event was then focused with an opposing doublet (f = 200 mm) onto the imaging sensor of a high-speed CMOS camera. Data was recorded at a resolution of 128 × 128 pixels with a 30 mm field of view at 90,000 fps (11 μsec interval between frames) using camera controller software.

Electrophysiological recording

Functional assessment of excised spinal cords was achieved by measuring the production of compound action potentials (CAPs) using a double-sucrose gap recording chamber. CAPs represent the spatial-temporal summation of all evoked potentials and were recorded before and after blast exposure. (Fig. 1C) The amplitudes of CAPs were measured 30 min after blast exposure to allow for complete recovery and compared to pre-injury baselines. Decreases in CAP amplitude are associated with functional deficits.

Ventral white matter strips were placed across the chamber with the middle of the cord housed in the central compartment under constant perfusion by oxygenated Krebs solution maintained at 37°C, while either end of the cord rested in the side compartments containing isotonic KCl (120 mM). Both gaps separating the side compartments from the central portion were perfused with sucrose (320 mM) to avoid ion exchange. One end of the cord was stimulated with a 0.3 V constant voltage pulse every 3 sec and the corresponding CAPs were recorded from the distal end using Ag-AgCl electrodes. Data were recorded using a bridge amplifier and

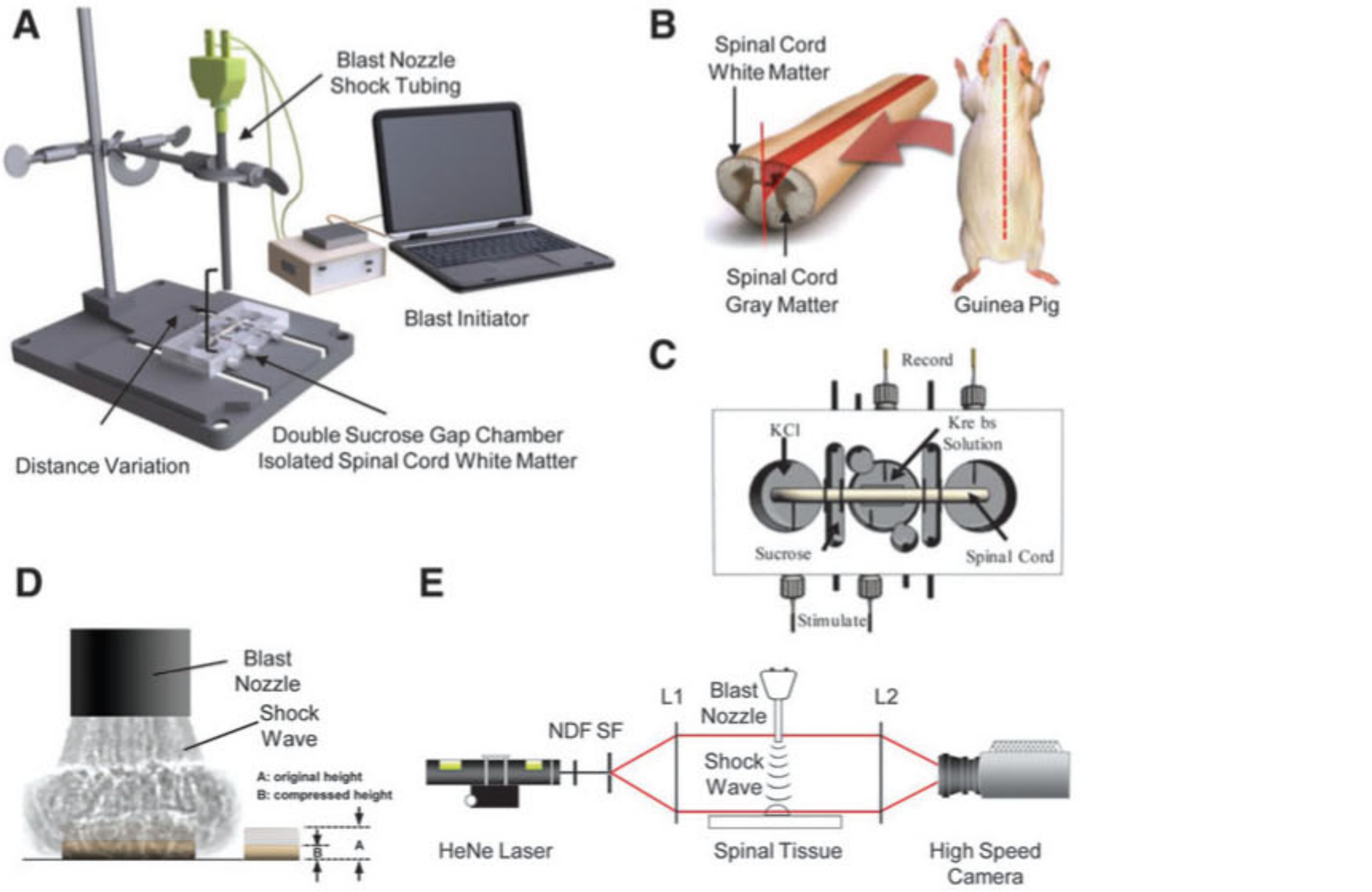

FIG. 1. Composite illustration of the experimental set-up. (**A**) Isolated spinal cord secured in the double-sucrose gap chamber was exposed to varying degrees of blast injury. Small-scaled explosive shock tubing housed in an aluminum nozzle was detonated using a custom remote initiator. Various degrees of exposure intensity were created by altering the distance between the end of the nozzle and the tissue sample according to Hopinkson's rule. (**B**) Diagram showing isolation of guinea pig spinal cord white matter. Whole cord was excised from the vertebral column and the white matter was collected. (**C**) Functional deficits were monitored by recording the production of compound action potentials (CAPs) using a double-sucrose gap chamber. Diagram depicts a top view of the chamber. Isotonic sucrose was perfused through the double gaps to separate isotonic KCl from the oxygenated Krebs solution cycling through the central chamber. The proximal end of the cord was stimulated and the CAPs were recorded on the distal end. (**D**) Representation of isolated spinal cord white matter deforming in response to blast injury. The explosion and resultant shockwave are directed along a hollow aluminum blast nozzle directly over the tissue sample. (**E**) Schematic of focused shadowgraphy. A HeNe laser light source was attenuated (neutral density filter, NDF) and filtered (spatial filter, SF) before being collimated and focused using an opposing pair of doublets (L1, L2, f=200 mm) onto the imaging sensor of a high-speed camera. Color image may be found at www.liebertpub.com/neu

processed with custom LabVIEW software (National Instruments Corp., Austin TX). A detailed description of the construction and dimensions of the chamber are reported in previous studies (Shi and Blight, 1996, 1997).

Membrane integrity

The HRP exclusion assay was performed as previously described to quantify the degree of anatomical damage resulting from membrane damage. Immediately following exposure to blast injury, the ventral white matter strips were transferred into oxygenated Krebs solution containing 0.015% HRP for 1 h before being placed in a 2.5% glutaraldehyde solution in phosphate buffer for 2 h. Treated spinal cords were then cut into 30-μm transverse sections at the injury epicenter using a vibratome. The sections were processed with diaminobenzidine (DMB) to visualize the degree of HRP uptake in damaged axons. Digital images of HRP-stained sections were captured using an optical microscope. Total numbers of stained axons were quantified using digital image software (Adobe Photoshop 7.0 and ImageJ), and results were expressed as mean density (axons/mm^2). Density calculations were performed using a normalization value of 4300 axons/mm^2 as the total number of axons in guinea pig spinal cord white matter permeable to HRP, as previously determined (Shi and Borgens, 2000).

Statistical analysis

Statistical significance was determined using one-way analysis of variance (ANOVA) with subsequent pair-wise comparisons performed using Tukey-Kramer HSD (unless otherwise noted) with significance level set at $p<0.05$. Values are reported as means ± standard error.

Results

Blast metrics

Detonation of the explosive produced a shockwave visualized in the shadowgrams shown in Figure 2A. Expansion of the shockwave circumferentially from the epicenter generated a subsequent region of underpressure referred to as the blast wind. The shockwave reached supersonic speeds in excess of 1100 mph (traveled 30 mm in approximately 56 μsec).

Distinct levels of blast intensity were created by varying the distance between the blast nozzle and the sensor to demonstrate

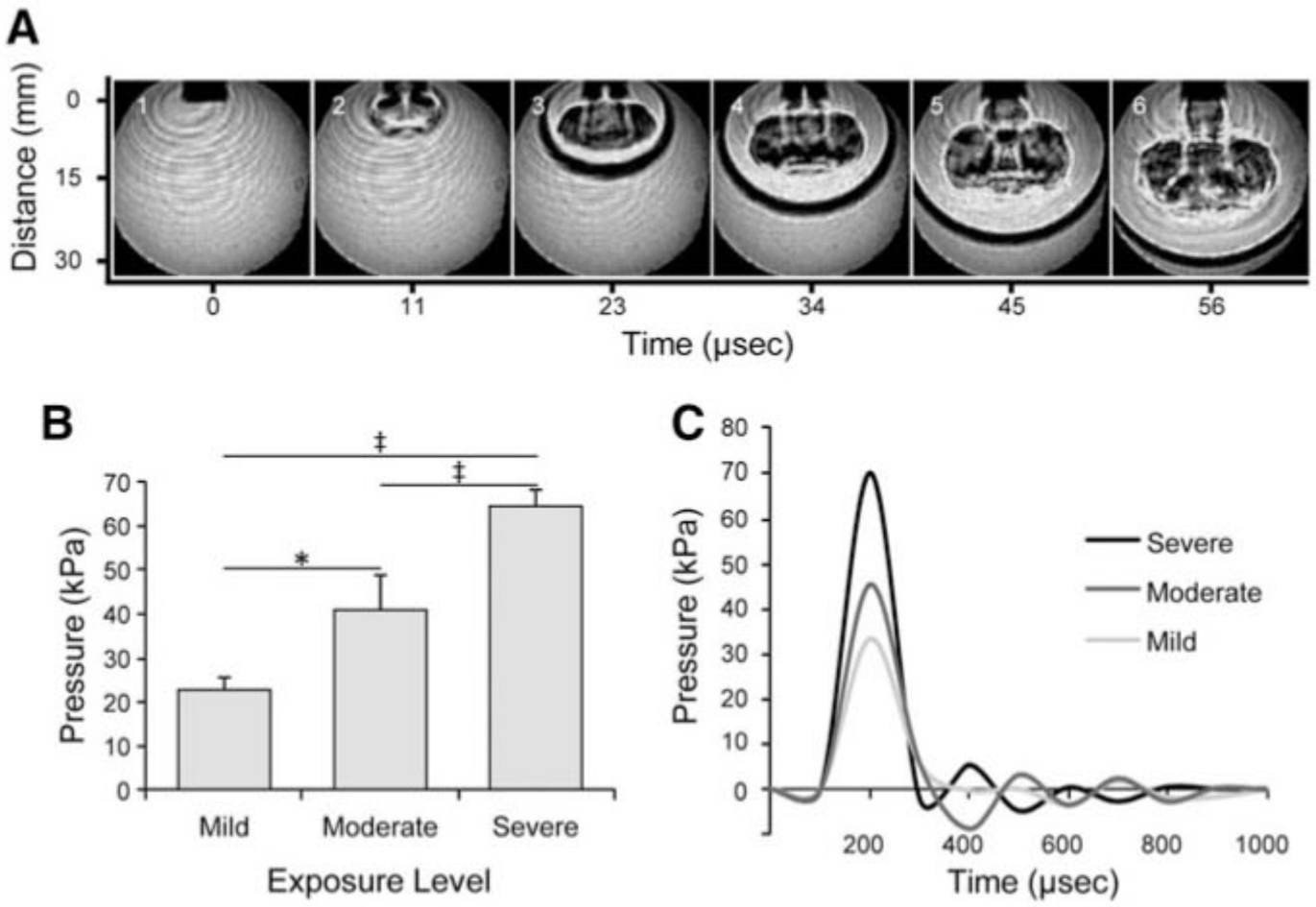

FIG. 2. Blast measurements. (**A**) Focused shadowgrams depicting the aluminum blast nozzle, and emergence and propagation of the supersonic shockwave and blast wind generated from detonating the small-scale explosive. (**B**) Total pressure recorded with a pressure transducer mounted normal to the propagating shockwave quantified peak overpressure for three levels of intensity. Mild, moderate, and severe exposure levels were achieved by decreasing the distance between the blast nozzle and the mounted sensor from 1.75 cm to 1.5 cm and 1.25 cm for each level, respectively. Mild exposure reached an average overpressure of 23 ± 1.67 kPa, moderate exposure achieved 41.15 ± 3.23 kPa, and severe exposure attained 64.74 ± 1.19 kPa (*significance at $p < 0.05$; ‡significance at $p < 0.01$; $n = 7$). (**C**) Representative pressure-time histories for the three exposure levels demonstrate a near instantaneous rise in overpressure with uniform impulse durations (200 μsec), followed by a decaying curve and region of underpressure. Pressure-time histories signify that small-scale explosives generate an ideal blast wave similar to the classical free-field Friedlander waveform.

the effects of blast loading on exposed nervous tissue and develop a dose-response curve. Exposure levels were designated as severe (1.25 cm), moderate (1.5 cm), and mild (1.75 cm), to achieve significantly different levels of overpressure. Average overpressure values are shown in Figure 2B. Severe exposure produced a blast pressure of 64.74 ± 1.19 kPa, moderate exposure attained 41.15 ± 3.23 kPa, and mild exposure averaged 23 ± 1.67 kPa. Representative pressure-time histories for each level are depicted in Figure 2C. The duration of the blast wave was approximately 200 μsec for each exposure level. Altering the blast overpressure did not significantly change the blast wave duration. Waveforms exhibit an idealized free-field Friedlander waveform characteristic of large-scale explosions (Stuhmiller et al., 1991).

Tissue loading

Determining the mechanical response of the tissue to blast loading was accomplished by directing a severe-level shockwave onto the isolated section of spinal cord. Resultant tissue deformation was visualized using focused shadowgraphy to capture the event shown in Figure 3A. The series of shadowgrams show charge detonation (frame 1, $t = 0$ μsec), wave propagation from the nozzle (frame 2, $t = 11$ μsec and frame 3, $t = 23$ μsec), impact with tissue (frame 4, $t = 34$ μsec), rapid deformation in response to loading (frame 5, $t = 45$ μsec and frame 6, $t = 55$ μsec) and unloading.

Percent deformation of the sample over the time course of detonation and impact is shown in Figure 3B. Maximum rate of deformation occurs immediately following the impact, achieving 50% compression of the tissue in 11 μsec. Deformation continues for an additional 11 μsec, reaching 60% compression before the shockwave dissipates. After exposure, the tissue returns to equilibrium over the course of 45 μsec at a rate of 29.3 m/sec. The rate of initial compression was determined to be 60 m/sec, and was calculated using 60% of the height of the spinal cord (1.32 mm) under a time course of 22 μsec. The corresponding strain rate was calculated as 18,181.82/sec.

Functional deficits

Functional deficit in response to primary blast injury was determined by measuring the loss of axonal conduction, which was in turn determined by comparing CAP amplitudes of post-injury 30 min after recovery with pre-injury baselines. Increased blast intensity produced by each of the three exposure levels correlated with increased functional loses. Specifically, control uninjured spinal cord exhibited a less than 1% reduction in amplitude over the experimental time course. Exposing the spinal cord sample to a mild, moderate, and severe blast reduced the CAP amplitude by $17.7 \pm 6.08\%$, $37.12 \pm 3.37\%$, and $56.24 \pm 4.52\%$, respectively. Instantaneous post-injury CAP waveforms after recovery for each exposure level are shown in Figure 4B. Increasing the severity of the exposure substantially decreases functional capacity in a linear relationship.

Anatomical deficits

Membrane permeability measured with the HRP-exclusion assay was used to quantify anatomical deficits in response to

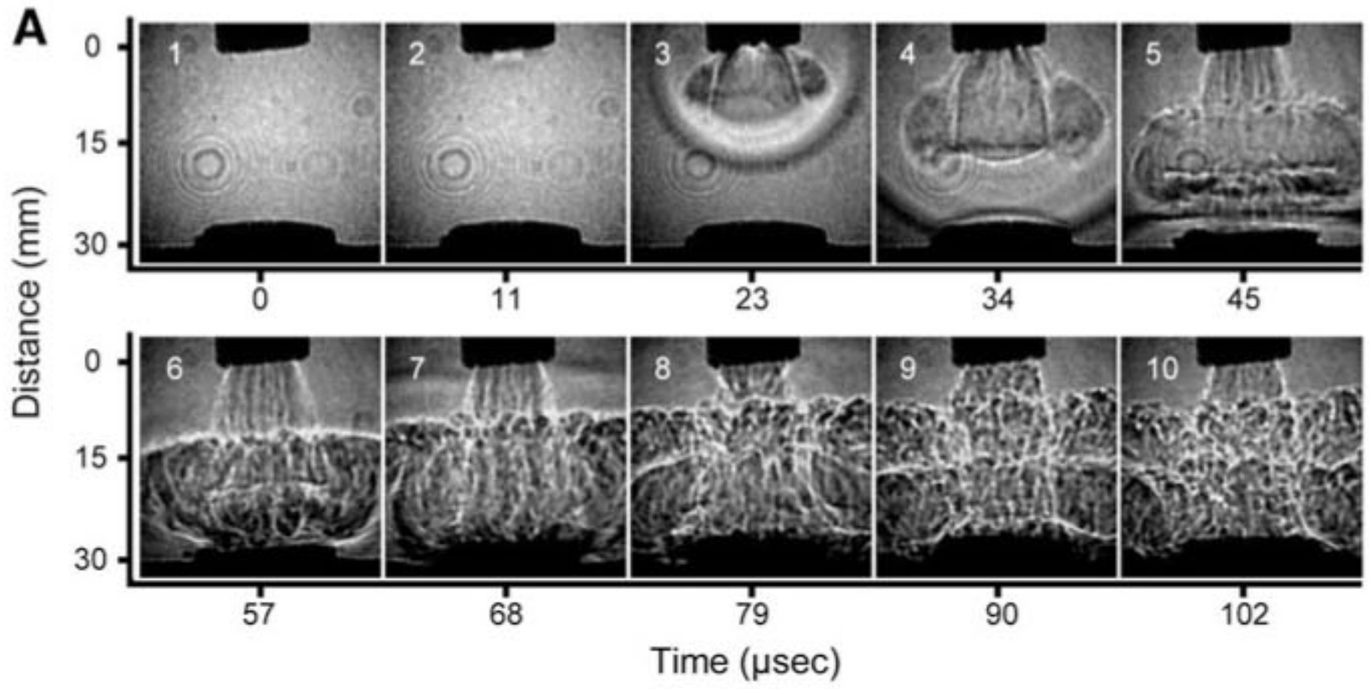

FIG. 3. Deformation of the spinal cord in response to the shockwave impacting the tissue. (**A**) Focused shadowgrams showing the blast nozzle, emergent shockwave, and section of spinal cord tissue secured to the substrate. Shadowgrams depict propagation of the supersonic shockwave (frames 1–3), impact with the spinal tissue (frame 4), resultant tissue deformation (frames 5–6), and return to equilibrium (frames 7–10) in response to blast loading. (**B**) Relative deformation of the spinal cord tissue sample. Maximum strain rate occurs between frames 4 and 5 at a rate of 60 m/sec, with maximum strain magnitude of 60% compression occurring at frame 6 before returning to equilibrium at a rate of 29.3 m/sec.

blast exposure. Representative photomicrographs are shown in Figure 5A, depicting the overall trend of increasing membrane permeability in response to increased blast exposure. Analysis, shown in Figure 5B, of the photomicrographs demonstrates increase an in permeability between exposure levels. Mild blast exposure significantly increased permeability to $7.83 \pm 1.39\%$ from $0.17 \pm 0.05\%$ in uninjured control samples. Increasing blast intensity to moderate and severe blast further increased membrane permeability to $24.67 \pm 5.5\%$ and $64.96 \pm 10.16\%$, respectively. Overall, the findings demonstrate that the severity of blast exposure is correlated with the degree of structural deficits marked by acute membrane permeability.

Discussion

Modern military conflicts have encouraged a resurgence in the study of blast injury. Continuing terrorist activity and increased use of explosive devices have led to a prominent increase in blast-related injuries (Coupland and Meddings, 1999; Warden, 2006; Warden et al., 2009). Despite the impact and interest of BINT, the mechanism of injury is still not well understood, in large part due to the limitations of the method of experimental models. Current animal models offer an understanding of the global response to blast exposure, but present several limitations. For instance, direct damage inflicted by the primary blast wave on the central nervous system is masked by confounding secondary systemic responses. As previously suggested, the circulatory and pulmonary systems potentially produce ischemic conditions or air emboli that indirectly contribute to blast-induced brain injury (Moore et al., 2008). Other suggestions include the indirect transfer of a pressure wave to the brain via the great vessels of the circulatory system (Bhattacharjee, 2008). Therefore, isolating the direct effects of blast exposure from secondary systemic contributions is critical in order to decipher the mechanism of injury and contribution of the blast wave to observed deficits following blast exposure.

The small-scaled experimental BINT model developed in this study is capable of uniquely separating the primary blast event from the confounding systemic response. We are able to create a supersonic blast wave with an epicenter diameter on the scale of centimeters. This small-scale explosive allows for repeatability in a highly controlled setting and precision for direct focus on isolated tissue samples. The model provides the capability of using battlefield related-explosives that offers a great deal of relevance (Stuhmiller et al., 1991). Detailed observation of both the blast wave and resulting tissue deformation was accomplished using a high-speed focused

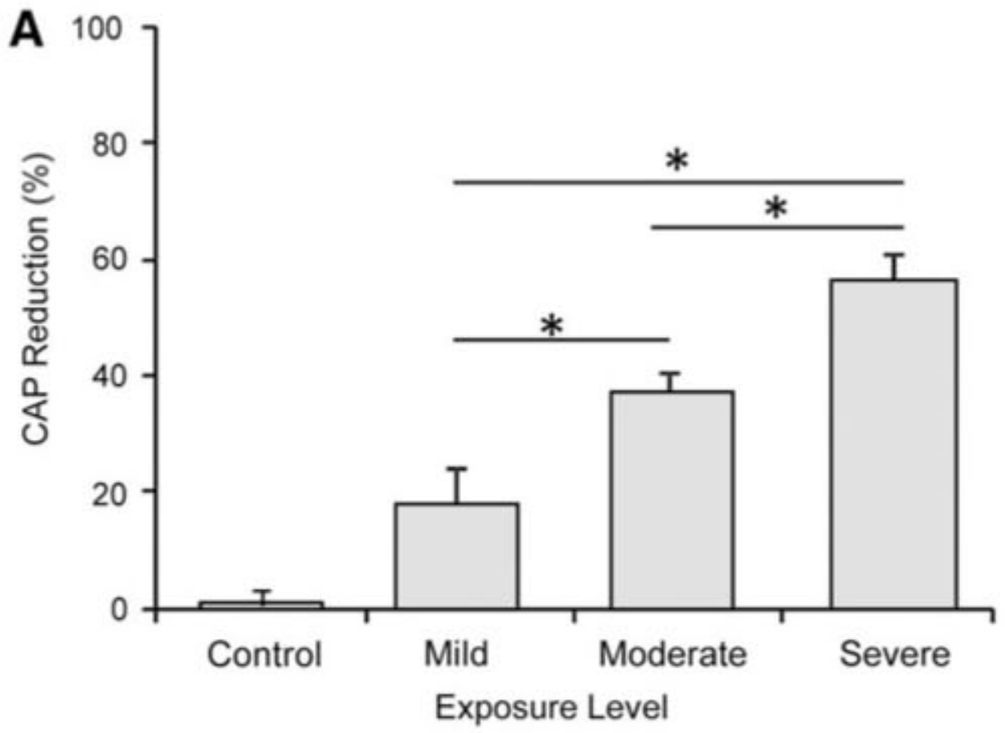

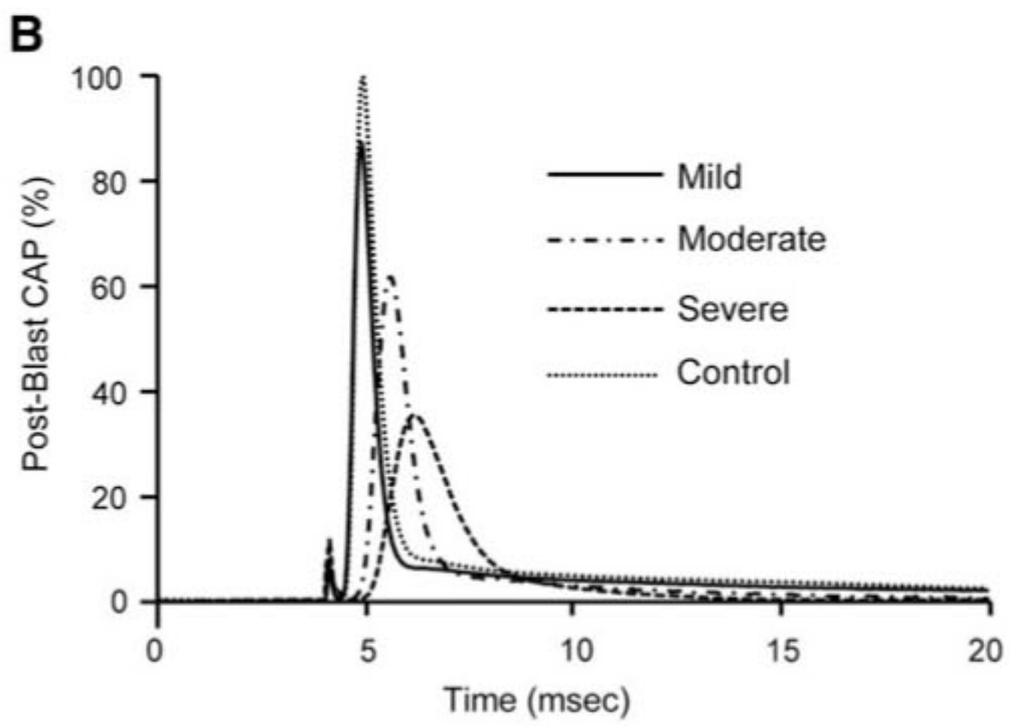

FIG. 4. Functional deficits in response to blast loading typified by loss in conduction of action potentials (CAPs). (**A**) Average percent reduction in CAPs by comparing post-blast measurements after sufficient recovery with pre-blast baseline. Increased blast intensity impairs conduction. Mild exposure decreased conduction by 17.7±6%, moderate exposure resulted in a 37.1±3.4% reduction, while severe exposure resulted in maximum functional deficits with a CAP reduction of 56.2±4.5%. (*significance at $p<0.05$). All treatment groups are significantly different from controls at $p<0.05$ ($n=4$). (**B**) Representative CAP waveforms for each exposure level demonstrating loss in amplitude along with increased latency, indicating that the total number of axons capable of conducting an action potential decreased with increasing severity of blast exposure.

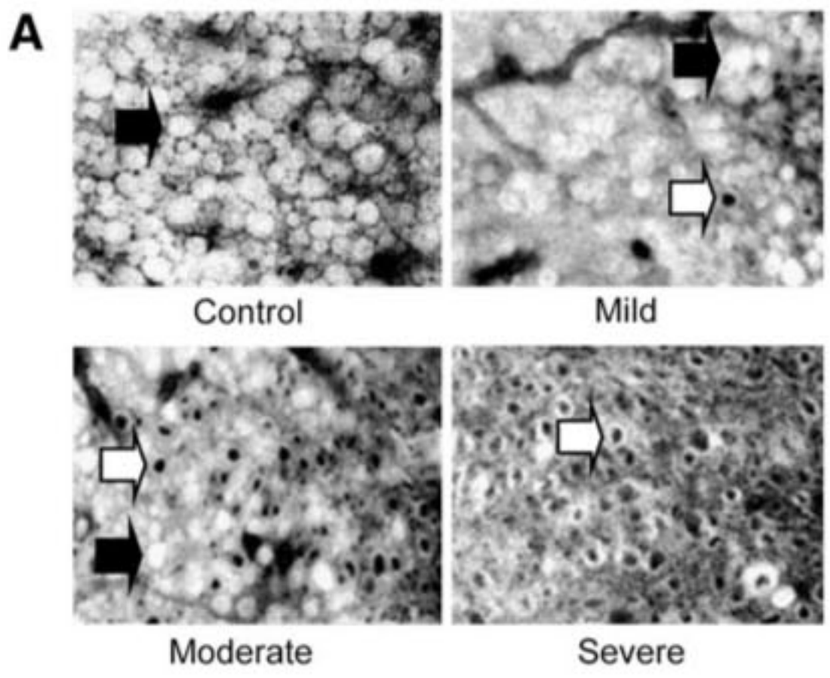

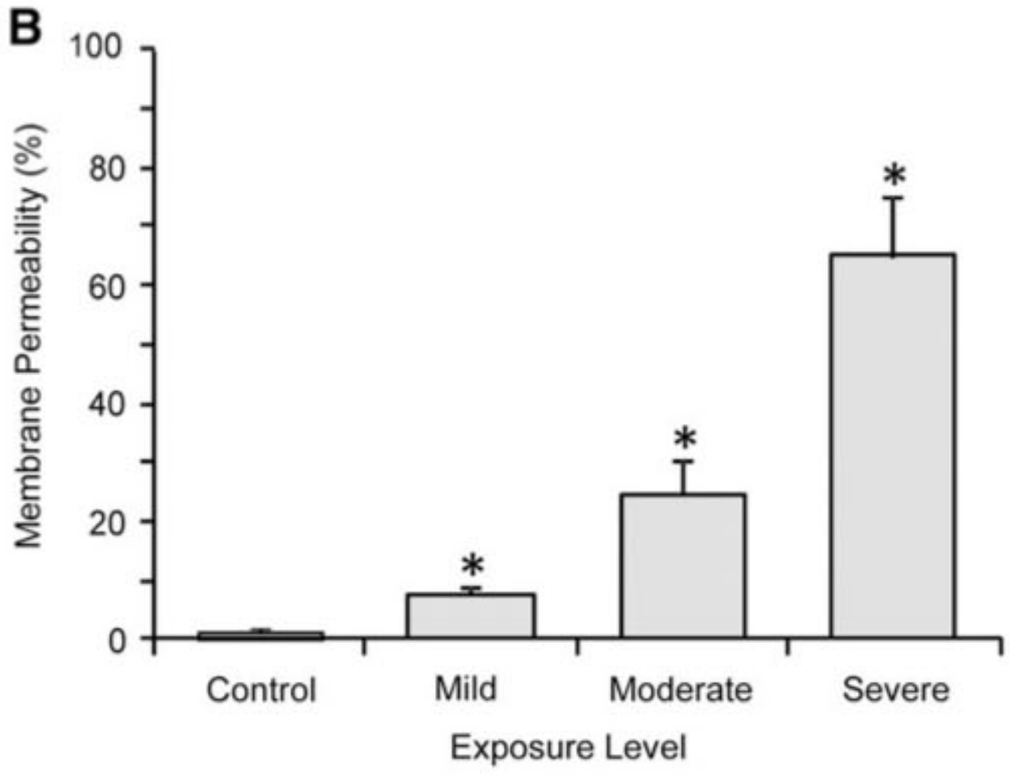

FIG. 5. Anatomical deficits in response to blast loading typified by a decrease in membrane integrity. (**A**) Representative photomicrographs of the HRP dye-exclusion assay demonstrating increased axonal permeability with increased blast severity. Black arrows denote damaged axons (HRP dye uptake), while white arrows indicate undamaged axons (HRP dye excluded). (**B**) Percent membrane permeability in response to increasing levels of blast exposure intensity (*significance from control at $p<0.05$ based on Kruskal-Wallis one-way analysis of variance; $n=4$–8).

shadowgraph technique (Figs. 2 and 3). Additionally, the model simultaneously recorded axonal function and correspondent axonal structural damage. To our knowledge, this is the first time a multimodal *ex vivo* model has been assembled to study blast-related nerve injury.

Additionally, our model uses isolated sections of guinea pig spinal cord tissue with known simple geometric properties. This greatly enhances the simplicity and accuracy of quantifying tissue deformation. We believe the isolated sections of spinal cord provide knowledge that can be applied to the brain. Spinal cord tissue closely models the cellular structure and mechanical properties of the brain. Complex geometric attributes of brain matter have traditionally made estimating tissue deformation complicated, while isolated spinal cord offers a simpler model for estimates.

We also believe our *ex vivo* model has advantages over many monolayer tissue culture preparations. For example, spinal cord tissue samples used in our model closely mimics *in vivo* parameters by preserving the local environment, unlike monolayer structures. Maintaining the local extracellular environment is critical, as the physical structure of the tissue greatly influences deformation and injury parameters. Our approach, therefore, maintains the simplicity of isolated models, while preserving critical physical characteristics for greater physiological relevance. Furthermore, the use of spinal cord tissue allows functional deficits to be simultaneously measured during blast exposure. Measurement of functional deficits can then be correlated to structural damage of the underlying tissue. Precise monitoring of the production of CAPs during blast exposure has not been reported in global animal models or in isolated brain slices.

Using this model, we examined the propagation of the blast wave using a focused high-speed (90,000 fps) shadowgraph technique, which allows for high resolution and sequential illumination of blast wave metrics. In the present report, we have characterized the blast wave profile, indicating that the wave travels at speeds in excess of 1100 mph and exhibits typical characteristics of an ideal free-field blast wave as witnessed on the battlefield (Stuhmiller et al., 1991). Furthermore, our high-frequency recording system adequately captures the necessary amount of frames to quantify the dynamics of tissue deformation during blast loading. We recorded one sample every 11 μsec to completely image the event lasting approximately 100 μsec (Fig. 3). Additionally, as shown in Figure 3A, the focused shadowgraph technique provides high-resolution images for precise measurement of tissue deformation. Based on our study, the blast wave compressed tissue at a rate of 60 m/sec with a corresponding strain rate of approximately 18,000/sec. This strain rate is orders of magnitude faster than the strain rate measured for traditional blunt impact traumatic brain injury (Bain and Meaney, 2000; Bayly et al., 2006; Geddes et al., 2003). Therefore, the strain rate in BINT may be an important difference from traditional traumatic injuries in the central nervous system.

Previous studies indicate that the rate of deformation plays a critical role in injury severity in addition to the magnitude of compression (LaPlaca et al., 1997; Shi and Whitebone, 2006). For instance, studies conducted on *ex vivo* spinal cord samples demonstrated that 60% compression at a measured rate of 0.05 mm/sec yields only a 2% reduction in CAP amplitude (Ouyang et al., 2009). In the present study, severe blast loading produced a 60% compression at a rate of 60 m/sec with a resulting 60% reduction in conduction. Comparing these two studies, the magnitude of compression remains constant, but increasing the rate of deformation significantly alters the functional capacity. Specifically, increasing the rate of deformation by several orders of magnitude from 0.05 mm/sec to 60 m/sec resulted in the CAP deficit increasing from 2% to 60%. The relation between the increasing rate of deformation and the loss of function is most likely not linear. Nervous tissue could be more sensitive to changes in rate at higher levels of rate. Based on these findings, we postulate that the dominant factor contributing to BINT injury could be the degree of strain rate rather than the magnitude of compression.

Our findings suggest that damage to the central nervous system from blast exposure could primarily occur by the blast wave compressing nervous tissue under high strain rates. Rapid compression of nervous tissue leads to decreased conduction capacity, marked by structural damage to the axonal membrane that produces increased permeability. We found that increasing the severity of blast exposure produced correspondent levels of functional and structural deficits in neural tissue.

Although the rate of compression is many orders of magnitude greater in BINT, the underlining mechanism of injury is potentially similar to traditional blunt impact neurotrauma. The primary blast wave produces similar mechanical injury by compressing tissue with high strain rates, and producing axonal membrane disruption. Increased non-selective permeability through damaged axonal membranes permits ion leakage that disrupts concentration gradients and contributes to axonal conduction failure (Ouyang et al., 2008; Shi and Whitebone, 2006; Simon et al., 2005,2007,2009). Similarly to blunt trauma, mechanical injury in blast trauma could also trigger a number of delayed secondary injury processes that exacerbate the effects of the primary injury. These pathological processes could contribute to the observed cognitive and behavioral deficits in BINT. Illuminating similarities between traditional blunt injuries and BINT could facilitate the development of treatment protocols for blast injury. Specifically, several effective treatments concerning spinal cord injury such as membrane resealing may also be useful in treating BINT. For example, polyethylene glycol (PEG), a hydrophilic polymer, has been shown to repair membrane damage, prevent secondary injury, and enhance structural and functional recovery following mechanical trauma (Luo and Shi, 2007; Shi and Borgens, 1999,2000). We envision that this treatment will also be effective in treating BINT, as severe membrane damage has also been detected in blast injury.

The rate of tissue deformation is most likely related to the blast wave duration (Fig. 2). Therefore, our model provides the ability to record strain rate as a function of duration associated with the shock wave. Acquiring additional information about the shock wave and relating that to the severity of injury could be useful to diagnose afflicted soldiers on the battlefield. For instance, military helmets could be modified to acquire vital data points using sensors for immediate diagnosis of injury. Future studies could be designed to correlate blast metrics such as overpressure and duration with functional deficits. Such studies will help to establish a comprehensive approach to determine the overall outcome of tissue damage due to blast exposure.

In conclusion, we believe this study provides insight into the mechanism of BINT by isolating the contribution of the blast wave on nerve tissue deformation under rapid strain rates, and directly inhibiting functional capacity while increasing axonal membrane permeability. This information can contribute to the development of failure criteria for accurate diagnosis and be used as a critical tool for developing protective equipment to mitigate blast injury.

Acknowledgments

The authors would like to thank Michel Schweinsberg for providing the graphical illustrations.

Author Disclosure Statement

No competing financial interests exist.

References

Bain, A.C., and Meaney, D.F. (2000). Tissue-level thresholds for axonal damage in an experimental model of central nervous system white matter injury. J. Biomech. Engineering-Transact. ASME 122, 615–622.

Bayly, P.V., Black, E.E., Pedersen, R.C., Leister, E.P., and Genin, G.M. (2006). In vivo imaging of rapid deformation and strain in an animal model of traumatic brain injury. J. Biomechanics 39, 1086–1095.

Bhattacharjee, Y. (2008). Neuroscience. Shell shock revisited: solving the puzzle of blast trauma. Science 319, 406–408.

Cernak, I., Wang, Z., Jiang, J., Bian, X., and Savic, J. (2001a). Cognitive deficits following blast injury-induced neurotrauma: possible involvement of nitric oxide. Brain Inj. 15, 593–612.

Cernak, I., Wang, Z., Jiang, J., Bian, X., and Savic, J. (2001b). Ultrastructural and functional characteristics of blast injury-induced neurotrauma. J. Trauma 50, 695–706.

Chavko, M., Koller, W.A., Prusaczyk, W.K., and McCarron, R.M. (2007). Measurement of blast wave by a miniature fiber optic pressure transducer in the rat brain. J. Neurosci. Methods 159, 277–281.

Clemedson, C.J. (1956). Blast injury. Physiol Rev. 36, 336–354.

Coupland, R.M., and Meddings, D.R. (1999). Mortality associated with use of weapons in armed conflicts, wartime atrocities, and civilian mass shootings: literature review. Br. Med. J. 319, 407–410.

Geddes, D.M., Cargill, R.S., and LaPlaca, M.C. (2003). Mechanical stretch to neurons results in a strain rate and magnitude-dependent increase in plasma membrane permeability. J. Neurotrauma 20, 1039–1049.

Kocsis, J.D., and Tessler, A. (2009). Pathology of blast-related brain injury. J. Rehabil. Res. Dev. 46, 667–672.

LaPlaca, M.C., Lee, V.M., and Thibault L.E. (1997). An in vitro model of traumatic neuronal injury: loading rate-dependent changes in acute cytosolic calcium and lactate dehydrogenase release. J. Neurotrauma 14, 355–368.

Luo, J., and Shi, R. (2007). Polyethylene glycol inhibits apoptotic cell death following traumatic spinal cord injury. Brain Res. 1155, 10–16.

Moochhala, S.M., Md, S., Lu, J., Teng, C.H., and Greengrass, C. (2004). Neuroprotective role of aminoguanidine in behavioral changes after blast injury. J. Trauma 56, 393–403.

Moore, D.F., Radovitzky, R.A., Shupenko, L., Klinoff, A., Jaffee, M.S., and Rosen, J.M. (2008). Blast physics and central nervous system injury. Future Med. 3, 243–250.

Okie, S. (2005). Traumatic brain injury in the war zone. N. Engl. J. Med. 352, 2043–2047.

Ouyang, H., Galle, B., Li, J., Nauman, E., and Shi, R. (2008). Biomechanics of spinal cord injury: a multimodal investigation using ex vivo guinea pig spinal cord white matter. J. Neurotrauma 25, 19–29.

Ouyang, H., Galle, B., Li, J., Nauman, E., and Shi, R. (2009). Critical roles of decompression in functional recovery of ex vivo spinal cord white matter: Laboratory investigation. J. Neurosurg. Spine. 10, 161–170.

Saljo, A., Bao, F., Shi, J., Hamberger, A., Hansson, H.A., and Haglid, K.G. (2002). Expression of c-Fos and c-Myc and deposition of beta-APP in neurons in the adult rat brain as a result of exposure to short-lasting impulse noise. J. Neurotrauma 19, 379–385.

Settles, G.S. (2001). *Schlieren and Shadowgraph Techniques*. Springer-Verlag: New York.

Shi, R., and Blight, A.R. (1996). Compression injury of mammalian spinal cord in vitro and the dynamics of action potential conduction failure. J. Neurophysiol. 76, 1572–1580.

Shi, R., and Blight, A.R. (1997). Differential effects of low and high concentrations of 4-aminopyridine on axonal conduction in normal and injured spinal cord. Neuroscience 77, 553–562.

Shi, R., and Borgens, R.B. (1999) Acute repair of crushed guinea pig spinal cord by polyethylene glycol. J. Neurophysiol. 81, 2406–2414.

Shi, R., and Borgens, R.B. (2000). Anatomical repair of nerve membranes in crushed mammalian spinal cord with polyethylene glycol. J. Neurocytol. 29, 633–643.

Shi, R., and Whitebone, J. (2006). Conduction deficits and membrane disruption of spinal cord axons as a function of magnitude and rate of strain. J. Neurophysiol. 95, 3384–3390.

Shi, R. (2004). The dynamics of axolemmal disruption in guinea pig spinal cord following compression. J. Neurocytol. 33, 203–211.

Simon, C.M., Prado, G.R., and LaPlaca, M.C. (2005). Membrane compromise in neuronal somata after contusion spinal cord injury. J. Neurotrauma 22, 1173–1173.

Simon, C., Sharif, S., Tan, R., and LaPlaca, M. (2007). Acute spinal cord injury-induced plasma membrane damage. J. Neurotrauma 24, 1282–1282.

Simon, C.M., Sharif, S., Tan, R.P., and LaPlaca, M.C. (2009). Spinal cord contusion causes acute plasma membrane damage. J. Neurotrauma 26, 563–574.

Stuhmiller, J.H., Phillips, Y.Y., and Richmond, D.R. (1991). The physics and mechanisms of primary blast injury. In: *Conventional Warfare Ballistic, Blast, and Burn Injuries Textbook of Military Medicine*. Department of the Army, Office of The Surgeon General, Borden Institute.

Warden, D.L., French, L.M., Shupenko, L., Fargus, J., Riedy, G., Erickson, M.E., Jaffee, M.S., and Moore, D.F. (2009). Case report of a soldier with primary blast brain injury. Neuroimage 47, 152–153.

Warden, D. (2006). Military TBI during the Iraq and Afghanistan wars. J. Head Trauma Rehabil. 21, 398–402.

Address correspondence to:
Riyi Shi, M.D., Ph.D.
Department of Basic Medical Sciences
School of Veterinary Medicine
Purdue University
408 S. University Street
West Lafayette, IN 47906
E-mail: riyi@purdue.edu